DNA vaccination against membrane-bound Kit ligand: A new approach to inhibiting tumour growth and angiogenesis

DNA VACCINATION AGAINST mbKitL: A NEW APPROACH TO INHIBITING TUMOR GROWTH AND ANGIOGENESIS

Cristina Olgasi, Patrizia Dentelli, Arturo Rosso, Alessandra Iavello, Gabriele Togliatto, Valentina Toto*, Marcella Liberatore*, Giuseppina Barutello**, Piero Musiani*, Federica Cavallo**° and Maria Felice Brizzi°

Department of Medical Sciences, University of Torino, Italy

*Aging Research Centre, G. d'Annunzio University, Chieti, Italy

** Molecular Biotechnology Center, University of Torino, Italy

°Corresponding authors

Department of Medical Sciences

University of Torino,

Corso Dogliotti 14,

E-mail: mariafelice.brizzi@unito.it

Molecular Biotechnology Center,

University of Torino

Via Nizza 52

10126 Torino Italy

E-mail: federica.cavallo@unito.it

Word abstract: 174

Word count: 2483

Number of figures: 8

Running title: mbKitL vaccination hinders tumor angiogenesis and growth.

Key words: DNA vaccination, tumor angiogenesis, Akt, mbKitL.

ABSTRACT

A functional c-Kit/Kit ligand (KitL) signaling network is required for tumor angiogenesis and growth, and therefore the c-Kit/KitL system might well be a suitable target for the cancer immunotherapy approach. We herein describe a strategy that targets membrane-bound KitL (mbKitL) via DNA vaccination. The vaccination procedure generated antibodies which are able to detect mbKitL on human tumor endothelial cells (TECs) and on the breast cancer cell line: TSA. DNA vaccination, interferes with tumor vessel formation and transplanted tumor growth *in vivo*. Histological analysis demonstrates that, while tumor cell proliferation and vessel stabilization are impaired, vessel permeability is increased in mice that produce mbKitL-targeting antibodies. We also demonstrate that vessel stabilization and tumor growth require Akt activation in endothelial cells but not in pericytes. Moreover, we found that regulatory T cells (Treg) and tumor infiltrating inflammatory cells, involved in tumor growth and angiogenesis, were reduced in number in the tumor microenvironment of mice that generate anti-mbKitL antibodies. These data provide evidence that mbKitL targeted vaccination is an effective means of inhibiting tumor angiogenesis and growth.

INTRODUCTION

Complex tumor-microenvironment interactions are known to drive tumor progression[1]. Several cell types involved in these processes express c-Kit, the receptor for the c-Kit ligand (KitL), and these include endothelial cells (ECs) and pericytes[2,3]. KitL is expressed in two variants; a membrane bound (mbKitL) and a soluble (sKitL) form[4]. The soluble form contains an extracellular proteolytic cleavage site which permits the release of KitL from the cell surface[4]. Conversely, the spliced variant is not cleaved in humans and remains associated with the cell surface (mbKitL). mbKitL, unlike the soluble form which hastily activates the receptor and decays after prompt receptor internalization, induces a more persistent signal[5-6]. c-Kit binding to the mbKitL expressed by bone marrow (BM)-derived stromal cells (SCs), supports stem cell survival *in-vivo*[7]. Likewise, ~~the~~ mbKitL, expressed by tumor ECs (TECs)[8], is crucial for survival signals in tumor vasculature[9,10]. A substantial body of data corroborates the involvement of paracrine/autocrine stimulation, via the c-Kit/KitL system, in cancerogenesis[11]. Recently it has been shown that c-Kit grades breast cancer cells including cells from Brca1-mutation-associated breast cancer[12]. These observations support the fact that the c-Kit signaling network is crucial not only to hematopoietic and vascular cells, but also to transformed mammary epithelial cells, and thus makes this system an ideal target for unconventional therapeutic strategies.

Targeted therapies that specifically inhibit the molecules involved in tumor progression have already been exploited in clinical settings[13,14]. However, tumors that are initially responsive to targeted therapies generally acquire resistance[15]. Immunotherapies targeting neoplastic lesion driving antigens have offered an alternative option[16,17]. However, the rate of tumor growth often exceeds immune system capabilities and the tumor microenvironment does not allow the local recruitment of immune cells and orchestrates a number of immunosuppressive activities, including the recruitment of a specific subpopulation of CD4+/CD25+ T lymphocytes called regulatory T cells (Treg)[18]. In addition, other genetic and epigenetic changes in tumor cells (TCs) and in the

microenvironment commonly occur in advanced tumors following the initial genetic shift[16,17]. The adaptive immune response activated by vaccination against antigens expressed by a clinically evident tumor, is faced with genetic instability causing the selection of heterogeneous tumor clones and the reappearance of TCs that elude the immune system[16,17]. Therefore, targeting tumor antigens is unlikely to guarantee lasting tumor growth control. An alternative approach is the targeting of antigens expressed by SCs[19-21], crucial drivers of tumor drug resistance[22]. Therefore, if the target molecule expressed by TCs is also aberrantly expressed by SCs and contributes to tumor progression, immunotherapy approaches should be more effective.

The aim of this study is to investigate the impact of DNA mbKitL targeted vaccination on tumor angiogenesis and growth.

MATERIALS AND METHODS

Immunization. The human mbKitL cDNA sequence (membrane domain of the KitL) was amplified by PCR as a HindIII/XhoI fragment using the following primers; 5' AGC TAA ACGGAT TCG CCA CAC C 3' (sense) and 5' ATA CTC GAG CTA CCA GTA TAA GGC 3'(antisense). The resulting PCR product was verified by DNA sequencing and subcloned into the HindIII/XhoI restriction sites of a pVAX1 vector (Invitrogen, Carlsbad, CA, USA) to generate pVAX-mbKitL. 8-10-week old Balb/c mice (Charles River Laboratories, Calco, Italy) were immunized every two weeks for a total of three doses via i.d. injection of 25 μg of pVAX-mbKitL or the pVAX empty vector or left untreated as controls. The injection solutions were made up with 20 μl of 0.9% NaCl + 6 mg/ml polyglutammate. Immediately after the injection two 25-ms low voltage electric pulses were generated at the injection site. Pulse amplitude was set at 150 V and a 300 ms interval was used between the pulses. Two non-penetrating plates of 30 mm in linear length were connected to the electroporator (Cliniporator™, IGEA s.r.l., Carpi, Italy). Mice were treated in conformity with European Guidelines and policies as approved by the University of Turin Ethical Committee.

Tumor challenge. To assess the effects of DNA vaccination on tumor growth untreated, pVAX and pVAX-mbKitL vaccinated mice were inoculated s.c. with $5x10^5$ TSA cells. Tumor size was measured every 3-4 days and calculated using the formula; $V=4/3\pi\times(d/2)^2\times(D/2)$ (d=minor tumor axis; D=major tumor axis) and reported as tumor mass volume (mm^3, mean ± SEM of individual tumor volume/each mouse per cohort) obtained after 35 days. Mice were killed when the tumor exceeded 800 mm^3 [23]. Log-rank test/Kaplan-Meier survival plots for this study display the probability of survival as the percentage of mice whose tumors did not exceed 2000 mm^3 on the indicated days.

Histology, immunohistochemistry and immunofluorescence. Cryostatic sections of tumor samples were stained with hematoxylin/eosin while others were processed for immunohistochemistry or for immunofluorescence to evaluate; vessel and pericyte staining,

microvessel and pericyte counts, in-situ proliferating cells, inflammatory cell and T-reg infiltration and vessel permeability.

EC and tumor cell isolation from tumor masses ~~and~~, mouse liver and spleen. Tumor samples were minced, digested and forced through a graded series of meshes to separate the cell component from stroma and aggregates. ECs were isolated by magnetic cell sorting using an anti-mouse CD31 antibody (MACS system, Miltenyi Biotech, Auburn, CA)[24,25]. The positive fraction corresponded to ECs, while the negative one mainly composed of TCs as denoted the CD31 negative fraction. Both cell populations were used for qRT-PCR and Western Blot (WB). The endothelial phenotype was verified by qRT-PCR and by WB for Flk1 expression. Vaccinated and tumor challenged mice were also subjected to liver and spleen explantation in order to recover ECs.

Adhesion assay. Adhesion of c-Kit-expressing cells (mouse BM-MNCs) to mbKitL-expressing cells (BM-SCs) was assayed in static conditions as previously described[7]. Briefly, BM-MNCs were labeled with the red fluorescent PKH26 vital dye and, after centrifugation at 1400 g for 10 min, were re-suspended in free medium containing 0.25% BSA. Cells were then added ($2x10^5$ cells/well) to a confluent monolayer of BM-SCs. In selected experiments BM-SCs were pre-treated with the sera derived from pVAX and pVAX-mbKitL vaccinated mice or with the anti-mbKitL antibody before the addition of BM-MNCs. Co-cultures were thus incubated at 37°C for 4h and non-adherent cells were removed by washing them three times with phosphate-buffered saline. To evaluate whether sera from pVAX-mbKitL vaccinated mice interfered with the adhesion of c-Kit expressing cells to stromal cells, BM-MNCs were allowed to adhere to BM-SCs for 4 hours and then incubated for 24h with sera. Samples were then fixed with 4% formaldehyde/ phosphate-buffered saline and observed under an epifluorescence microscope. Bound labeled c-Kit expressing cells were counted by three different operators in triplicate and reported as number ± SEM of adherent cells per field (10 fields at 20X magnification per sample).

Statistical Analysis. Data are representative of at least three independent experiments, performed in triplicate, unless otherwise indicated. Densitometric analysis was used to calculate the differences in

the fold induction of protein levels (relative amount), normalized as indicated *(*p< 0.05, **p<0.01, ***p<0.001*, statistically significant). Western blot panels and relative densitometric histograms are representative of the results obtained by replicates performed in triplicate (*n*=3 or *n*=4 or n=5). The significance of the differences between experimental and control values *(*p< 0.05, **p<0.01, ***p<0.001*) was calculated using variance analysis with Newman-Keuls multi-comparison tests. The differences in tumor-free survival (plotted as % tumor-free mice) were evaluated using the log-rank test/Kaplan-Meier survival plots.

Details of each experimental procedure are reported in the SI.

Reagents and Antibodies, Cell cultures and proliferation, Cytofluorimetric analysis, In-vivo angiogenesis, Tube-like structure formation, Vessel permeability, siRNA technology and cell transfection, ELISA assays, Analysis of the medullar component, Western blot, Immunoprecipitation experiments, Cytotoxicity test, RNA isolation and Real-Time Polymerase Chain Reaction (RT-PCR), Wound healing model are all reported in the SI.

RESULTS

mbKitL DNA vaccine

The pVAX1 vector containing human mbKitL cDNA was generated (pVAX-mbKitL, Fig. 1A). mbKitL protein expression was confirmed via transient transfection into CHO cells (Fig. 1B). Balb/c mice were vaccinated with pVAX-mbKitL or the empty-vector. To assess antibody response, sera were collected and analyzed by FACS on mouse BM-SCs expressing mbKitL (Fig. S1A). As shown in Fig. 1C-D, pVAX-mbKitL vaccination induced anti-mbKitL antibodies in 66.6% of the pVAX-mbKitL vaccinated animals, while control mice were negative. Functional studies performed on BM-SCs (Fig. 1F-S2) demonstrated that, unlike sera from control mice, sera from anti-mbKitL antibody positive pVAX-mbKitL mice prevented c-Kit-expressing cells adhesion to BM-SCs. Immunoprecipitation studies performed on TSA cells using sera collected from pVAX and pVAX-mbKitL vaccinated mice confirmed the presence of specific anti-mbKitL antibodies (Fig. 1E). To exclude the possibility that these endogenously produced anti-mbKitL antibodies affect sKitL serum concentrations, we performed an ELISA assay. As shown in Fig. S1B, no differences in sKitL serum concentrations were detected in the various groups. Sera cytotoxicity was excluded by incubating BM-SCs with different serum concentrations. Trypan blue was used to assess cell viability (Fig. S1C).

Vaccination against mbKitL inhibits tumor growth

The effect exerted by DNA vaccination on tumor growth was evaluated by injecting syngeneic mammary cancer-derived TSA cells that express c-Kit and the two KitL isoforms into the mammary-fat-pads of previously immunized Balb/c mice[26,27] (Fig. S3A-C). Tumor growth was assessed twice a week for 35 days (Fig. 2A). Mice were sacrificed when tumors in the control group reached a size of at least 800 mm^3, apart from the animals (4-mice/group) which were monitored for tumor-free survival (Fig. 2B). Gross analysis (Fig. 2C) revealed that pVAX-mbKitL vaccinated mice that developed anti-mbKitL antibodies showed reduced tumor mass. Accordingly, the number of PCNA positive TCs was reduced in pVAX-mbKitL vaccinated mice (Fig. 3A). Similar results

were obtained in TSA cells which were cultured *in-vitro* with sera from pVAX-mbKitL animals (Fig. 3B). These data suggest that mbKitL targeted vaccination impairs tumor growth by interfering with tumor cell proliferation, as confirmed by knocking-down mbKitL on TSA cells *in-vitro* (Fig. S3D-E).

Tumors from animals that generate mbKitL-targeting antibodies displayed numerous areas of mostly central necrosis (Fig. 3D), while scant necrotic areas were found in empty-vector mice (Fig. 3C). Intra-tumor blood vessels were immature in both pVAX-mbKitL and control vaccinated mice, as suggested by the lack of α-SMA expression (Fig. S4). Nevertheless, vessels in pVAX-mbKitL mice displayed morphological alterations (Fig. 3F). They were wider and more irregular than vessels in control animals (Fig. 3E), and formed lacunae with a thrombi-free lumen. Their walls were almost entirely composed of ECs with scant and non-uniform pericytial cover (Fig. 3G-H). This vessel destabilization indicates increased vessel permeability. Functional studies performed with fluorescent microspheres administered 7 days after the last pVAX-mbKitL vaccination, show significant extravasation and trapping in the payload of tumor perivascular areas (Fig. 4A-C). Conversely, no extravasation was found in pVAX-vaccinated mice (Fig. 4D-F).

Foxp3-positive cells and F4/80-positive myeloid cells were fewer in number in tumors recovered from mice immunized against mbKitL (Fig. 4G-I). Western blot analysis and immunofluorescence experiments further confirmed the decreased number of Treg cells in pVAX-mbKitL animals (Fig. 4H-S5).

Tumors from pVAX-mbKitL mice that did not develop anti-mbKitL antibodies were similar to those from pVAX-vaccinated mice (not shown). Thus, data reported for pVAX-mbKitL mice will refer to mice that developed anti-mbKitL antibodies from here onward.

mbKitL-targeted vaccination impairs tumor vessel formation and VEGF bioavailability

As the effect of vaccination was evident on tumor vessels, we compared the expression of mbKitL on tumor-derived and normal ECs. Tumor-derived EC fraction purity was confirmed by Flk1 mRNA and protein expression (Fig. S6A-B). As shown in Fig. 5A-B, mbKitL was almost

undetectable on normal ECs, while it was evident on tumor-derived ECs. The effect of endogenously-produced mbKitL-targeting antibodies on vessel formation was then evaluated *in-vivo*. Human-derived TECs, expressing mbKitL and able to form neovessels *in-vivo*[8,10], were suspended in Matrigel and injected subcutaneously into SCID mice together with sera from pVAX or pVAX-mbKitL animals. Histological analysis of Matrigel plugs (Fig. 5C) revealed that the number of vessels formed by TECs was reduced when sera from pVAX-mbKitL mice was used.

VEGF production by TCs also contributes to tumor angiogenesis[28,29]. Data in Fig. 5D-E show that VEGF production by the tumor-derived $CD31^-$ fraction was impaired in pVAX-mbKitL mice. Similar results were obtained in TSA cells that were challenged *in-vitro* with sera from pVAX-mbKitL mice (Fig. 5F-G), suggesting that VEGF bioavailability might be reduced in the tumor microenvironment. STAT3 activation is crucial for HIF-1 expression and VEGF production in TCs as well as in ECs[30]. In fact, HIF-1 expression and STAT3 phosphorylation were reduced in tumors recovered from pVAX-mbKitL mice (Fig. S6C-D)

mbKitL targeted vaccination interferes with vessel stabilization

The finding that pericyte coverage was almost absent in tumor samples from pVAX-mbKitL mice (Fig. 3H), led us to investigate the underlying mechanisms. We first demonstrated mbKitL expression on pericytes (Fig. S7A-B). Based on this result, functional studies were performed on an *in-vitro* angiogenesis assay. Co-cultures of pre-labeled ECs and pericytes were performed in the presence of sera from vaccinated mice. As in the *in-vivo* results, no cordlike-structures with pericytes in close apposition could be detected when sera from pVAX-mbKitL animals were used (Fig. 6A).

In a different tumor model, Franco et al.[31] demonstrated that functional PDGFRs are required for proper pericyte/EC juxtaposition which ultimately leads to EC survival. However, when we assayed ECs or pericytes, which had been pretreated with imatinib mesylate or with an anti-PDGFR blocking antibody in co-culture experiments, EC/pericyte interaction was still

detectable (Fig 6B) suggesting that either c-Kit or PDGFR kinase activity is not relevant for EC/pericyte juxtaposition in our model. Imatinib mesylate, exploited in tumor-bearing mice, consistently failed to confer tumor protection and additional benefits when associated with pVAX-mbKitL vaccination (not shown).

Akt activation is required for tumor growth and EC/pericyte interaction.

As Akt activation is crucial for survival signals[6,7], we investigated whether mbKitL-targeting antibodies induced tumor growth inhibition by hampering Akt-mediated signals. As shown in Fig. 6C Akt activation was impaired in tumor-derived ECs and in the tumor-derived $CD31^-$ fraction recovered from pVAX-mbKitL vaccinated mice. Furthermore, *in-vitro* Akt activation was not detected in TSA cells and normal-ECs when sera from pVAX-mbKitL animals and the anti-KitL antibody (control) were used (Fig. 6D). Akt interference or TSA cells transfection with the Y719F c-Kit mutant[6,32] (Fig. S7C), which is unable to activate Akt, further validated Akt's contribution to TSA cell growth (Fig. S7D).

Considering Akt's crucial role in controlling c-Kit/mbKitL-mediated signals[6,7], Akt activation was evaluated on cell lysates from EC/pericyte co-cultures. Data in Fig. 7A demonstrate that only sera containing endogenously-produced mbKitL-targeting antibodies inhibit Akt activation. Moreover, functional studies performed with pericytes and Akt-depleted ECs demonstrated that Akt activation in ECs is essential for proper physical and functional pericyte/EC association (Fig. 7B).

Vaccination induced mbKitL antibodies have no effect on BM cell homeostasis and physiological angiogenesis.

The possibility that endogenously-produced antibodies may affect BM homeostasis[7] was evaluated. Fig 8A shows that sera from pVAX-mbKitL vaccinated animals did not interfere when an adhesion assay simulating stable adhesion between c-Kit expressing cells and BM-SCs was run. In addition, sKitL serum concentrations (Fig S1B) and the number of BM-derived-CFU-colonies

(Fig 8B) were similar in the two experimental groups. Finally, the physiological wound-healing process took place with similar efficiency in both pVAX and pVAX-mbKitL animals (Fig 8C).

DISCUSSION

The accumulation of genetic and epigenetic alterations in expanding tumors and immunosuppressive mechanisms activation by TCs and their microenvironment are known to drive tumor evasion and drug resistance[33], and highlight the need for novel anti-cancer strategies. The immunotherapy targeting of antigens involved in tumor progression and/or those abnormally expressed by SCs in the tumor microenvironment has provided new possibilities[16,17,33]. In this work, an mbKitL targeted immunotherapy approach demonstrates that transplanted tumor growth was impaired in mbKitL-targeting antibody generating mice. However, DNA electroporation, other DNA vaccination technologies[34] and more conventional vaccination approaches that induce a sustained antibody response[35] may well give similar results. It is conceivable that the vaccine-induced antibody effect may principally rely on tumor vascular growth inhibition; however, the decreased number of PCNA positive TCs detected in pVAXmbKitL vaccinated animals also hints at a direct tumor cell effect. Indeed, solid tumor formation is attenuated in transgenic mice that bear c-Kit kinase defective mutations (mice carrying *W* mutations)[11], and the survival/growth of tumor mammary epithelium requires a functional c-Kit[12]. As proof of concept, we found that: sera from pVAX-mbKitL vaccinated mice inhibited TSA cell expansion and reduced the number of PCNA positive cells *in-vitro*; Akt activation, crucial for survival signals elicited by the c-Kit/mbKitL interaction[5,6], was detected in TCs derived from pVAX but not from pVAX-mbKitL mice; TSA cell expansion was impaired by knocking-down mbKitL and Akt activation.

Tumor vasculature is a potential target because of its crucial role in tumor progression[36]. The present results demonstrate that vaccination causes a reduction in functional vessel numbers and a lack of proper pericyte coverage. The absence of pericytes on the vessel wall caused destabilization and enhanced permeability, as shown by selective microsphere extravasation. Moreover, blood stasis in the widened vessels may create an uncomfortable milieu for TCs, which explains necrotic areas found in pVAX-mbKitL vaccinated animals. Such an effect can also contribute to a decrease in TC proliferating activity.

Pericyte coverage was originally considered a vessel wall-stabilizing factor, thus assuring the proper distribution of chemotherapeutics inside tumors[36]. However, it has recently been reported that pericyte-covered vessels contribute to vascular targeting agent acquired resistance[22,31]. Although the association between pericytes and ECs has been extensively explored, the mechanics behind the crosstalk during physiological or tumor angiogenesis is not completely understood. We herein demonstrate that persistent Akt activation in ECs might contribute to the physical and functional EC/pericyte association in tumors. Furthermore, as in other models[37] c-Kit binding to its mbKitL, not its kinase activity, results in cell adhesion and survival[5,6] by maintaining stable Akt activation. This appears to be particularly true for ECs, as the knock down of Akt led to an impairment of tube-like-structure formation and pericyte coverage. Therefore, as in BM, where mbKitL supports long-term hematopoietic stem cell survival[7], mbKitL might sustain survival signals for vessels by preserving pericyte coverage in tumor vasculature.

The limited success of anti-angiogenic drug-based treatments in clinical trials seems to depend mainly on anti-VEGF-driven hypoxia, ultimately resulting in the expression of HIF-1 and/or HIF-1 related genes[38]. The finding that endogenously produced mbKitL-targeting antibodies inhibit tumor cell-derived VEGF, without promoting HIF-1 expression, is aligned with its inhibitory effect on tumor expansion. Vaccination negatively modulates a crucial determinant of the HIF-1 regulatory machinery, activated STAT3[30], which is consistent with the reduced expression of HIF-1. Thus, targeting mbKitL might confer additional therapeutic benefits.

A tumor microenvironment contains various cellular populations including T-reg cells and monocytes that, by influencing tumor immunosuppression and altering the quality of vessel, are crucial drivers of tumor progression[1]. Data have shown that targeting tumor-infiltrating macrophages by inhibiting chemokine (C-C motif) receptor 2 and colony-stimulating growth factor 1 receptor results in impaired monocyte recruitment from circulation and reduced tumor infiltrating monocyte/macrophage survival[39]. Our data did not provide insight into the mechanics of how vaccination against mbKitL interferes with T-reg and myeloid cell recruitment, nevertheless, as

these cells may promote the immune suppression shift by altering CD11b+Ly6G cell functional activities, it is conceivable that vaccination might contribute to reverting the immune balance shift.

Although long-standing anti-angiogenic memory generally raises relevant safety concerns, studies into immunotherapeutic approaches that target angiogenic proteins have not revealed any or only minor effects on physiological angiogenesis[19-21]. Similarly, deferred wound healing was not detected in our vaccinated mice. Additional safety concerns arise from the crucial role played by mbKitL in long-term BM-derived progenitor survival[7]. However, we failed to detect BM-failure in our vaccinated mice. Moreover, no change in sKitL serum concentrations were detected, indicating that endogenously-produced mbKitL-targeting antibodies were able to induce reasonable and balanced inhibition which offers a therapeutic advantage in treating cancers.

Tyrosine kinase receptor inhibitor-based therapies have shown partial clinical benefits in breast cancer patients[40]. The occurrence of drug resistance, mainly dependent on tumor stroma, is still the most challenging factor in cancer treatment efficacy[22]. The results of this study indicate that endogenously produced anti-mbKitL-antibodies inhibit tumor growth by targeting the tumor microenvironment. This suggests that exploiting vaccination in conjunction with chemotherapeutics, might avoid the emergence of drug resistance besides improving therapeutic outcomes.

ACKNOWLEDGEMENTS

This work was supported by grants from the Italian Association for Cancer Research (AIRC) to M.F.B (IG 5649) P.M. and F.C. (IG 5377) and by MIUR (Ministero dell'Università e Ricerca Scientifica) to M.F.B and P.M.

CONFLICTS OF INTEREST

The authors declare that no conflicts of interest exist.

REFERENCES

1. Balkwill F, Charles KA, Mantovani A. **Smoldering and polarized inflammation in the initiation and promotion of malignant disease**. *Cancer Cell*. 2005; 3: 211-217.
2. Aye MT, Hashemi S, Leclair B, Zeibdawi A, Trudel E, Halpenny M, Fuller V, Cheng G **Expression of stem cell factor and c-kit mRNA in cultured endothelial cells, monocytes and cloned human bone marrow stromal cells** (CFU-RF). *Exp Hematol*. 1992; 20(4): 523-527.
3. Wang CH, Verma S, Hsieh IC, Hung A, Cheng TT, Wang SY Liu YC, Stanford WL, Weisel RD, Li RK, Cherng WJ. **Stem cell factor attenuates vascular smooth muscle apoptosis and increases intimal hyperplasia after vascular injury**. *Arterioscler Thromb Vasc Biol.* 2007; 27(3): 540-547.
4. Huang EJ, Nocka KH, Buck J, Besmer P. **Differential expression and processing of two cell associated forms of the kit-ligand: KL-1 and KL-2**. *Mol Biol Cell*. 1992; 3(3): 349-362.
5. Miyazawa K, Williams DA, Gotoh A, Nishimaki J, Broxmeyer HE, Toyama K. **Membrane-bound Steel factor induces more persistent tyrosine kinase activation and longer life span of c-kit gene-encoded protein than its soluble form**. *Blood*. 1995; 85(3): 641-649.
6. Dentelli P, Rosso A, Balsamo A, Colmenares Benedetto S, Zeoli A, Pegoraro M, Camussi G, Pegoraro L, Brizzi MF. **C-KIT, by interacting with the membrane-bound ligand, recruits endothelial progenitor cells to inflamed endothelium**. *Blood*. 2007; 109(10): 4264-4271.
7. Slanicka Krieger M, Nissen C, Manz CY, Toksoz D, Lyman SD, Wodnar-Filipowicz A. **The membrane-bound isoform of stem cell factor synergizes with soluble flt3 ligand in supporting early hematopoietic cells in long-term cultures of normal and aplastic anemia bone marrow**. *Exp Hematol*. 1998; 26(5): 365-373.

8. Bussolati B, Deambrosis I, Russo S, Deregibus MC, Camussi G. **Altered angiogenesis and survival in human tumor-derived endothelial cells**. *FASEB J*. 2003; 17(9): 1159-1161.
9. Pan PY, Wang GX, Yin B, Ozao J, Ku T, Divino CM, Chen SH. **Reversion of immune tolerance in advanced malignancy: modulation of myeloid-derived suppressor cell development by blockade of stem-cell factor function.** *Blood*. 2008; 111(1): 219-228.
10. Dentelli P, Rosso A, Olgasi C, Camussi G, Brizzi MF. **IL-3 is a novel target to interfere with tumor vasculature.** *Oncogene*. 2011; 30(50): 4930-4940.
11. Li Q, Kondoh G, Inafuku S, Nishimune Y, Hakura A. **Abrogation of c-kit/Steel factor-dependent tumorigenesis by kinase defective mutants of the c-kit receptor: c-kit kinase defective mutants as candidate tools for cancer gene therapy**. *Cancer Res*. 1996; 56(19): 4343-4346.
12. Regan JL, Kendrick H, Magnay FA, Vafaizadeh V, Groner B, Smalley MJ. **c-Kit is required for growth and survival of the cells of origin of Brca1-mutation-associated breast cancer.** *Oncogene*. 2012; 31(7): 869-83.
13. Heath VL, Bicknell R. **Anticancer strategies involving the vasculature**. *Nat Rev Clin Oncol*. 2009; Jul;6(7):395-404
14. Arrondeau J, Gan HK, Razak AR, Paoletti X, Le Tourneau C. **Development of anti-cancer drugs**. *Discov Med*. 2012; 10(53): 355-362.
15. Broekman F, Giovannetti E, Peters GJ. **Tyrosine kinase inhibitors: Multi-targeted or single-targeted?** *World J Clin Oncol*. 2011; 2(2): 80-93.
16. Lollini PL, Cavallo F, Nanni P, Forni G. **Vaccines for tumour prevention**. *Nat Rev Cancer*. 2006; 6(3): 204-216.
17. Cavallo F, Calogero RA, Forni G. **Are oncoantigens suitable targets for anti-tumour therapy?** *Nat Rev Cancer.* 2007; 7(9): 707-713.
18. Colombo MP, Piconese S. **Regulatory-T-cell inhibition versus depletion: the right choice in cancer immunotherapy.** *Nat Rev Cancer.* 2007; 7(11): 880-887.

19. Niethammer AG, Xiang R, Becker JC, Wodrich H, Pertl U, Karsten G, Eliceiri BP, Reisfeld RA. **A DNA vaccine against VEGF receptor 2 prevents effective angiogenesis and inhibits tumor growth**. *Nat Med*. 2002; 8(12): 1369-1375.

20. Holmgren L, Ambrosino E, Birot O, Tullus C, Veitonmäki N, Levchenko T, Carlson LM, Musiani P, Iezzi M, Curcio C, Forni G, Cavallo F, Kiessling R. **A DNA vaccine targeting angiomotin inhibits angiogenesis and suppresses tumor growth**. *Proc Natl Acad Sci USA.* 2006; 103(24): 9208-9213.

21. Haller BK, Bråve A, Wallgard E, Roswall P, Sunkari VG, Mattson U, Hallengärd D, Catrina SB, Hellström M, Pietras K. **Therapeutic efficacy of a DNA vaccine targeting the endothelial tip cell antigen delta-like ligand 4 in mammary carcinoma**. *Oncogene.* 2010; 29(30): 4276-4286.

22. Cascone T, Herynk MH, Xu L, Du Z, Kadara H, Nilsson MB, Oborn CJ, Park YY, Erez B, Jacoby JJ, Lee JS, Lin HY, Ciardiello F, Herbst RS, Langley RR, Heymach JV. **Upregulated stromal EGFR and vascular remodeling in mouse xenograft models of angiogenesis inhibitor-resistant human lung adenocarcinoma**. *J Clin Invest*. 2011; 121(4): 1313-1328.

23. Uberti B, Dentelli P, Rosso A, Defilippi P, Brizzi MF. **Inhibition of β1 integrin and IL-3Rβ common subunit interaction hinders tumour angiogenesis.** *Oncogene.* 2010; 29(50):6581-90.

24. Dentelli P, Rosso A, Orso F, Olgasi C, Taverna D, Brizzi MF. **microRNA-222 controls neovascularization by regulating signal transducer and activator of transcription 5A expression.** *Arterioscler Thromb Vasc Biol*. 2010; 30(8):1562-8.

25. Togliatto G, Trombetta A, Dentelli P, Rosso A, Brizzi MF. **MIR221/MIR222-driven post-transcriptional regulation of P27KIP1 and P57KIP2 is crucial for high-glucose- and AGE-mediated vascular cell damage**. *Diabetologia* . 011; 54(7): 1930-40.

26. Musiani P, Modesti A, Giovarelli M, Cavallo F, Colombo MP, Lollini PL, Forni G. **Cytokines, tumour-cell death and immunogenicity: a question of choice**. *Immunol Today*. 1997; 18(1): 32-36.

27. Giovarelli M, Cappello P, Forni G, Salcedo T, Moore PA, LeFleur DW, Nardelli B, Di Carlo E, Lollini PL, Ruben S, Ullrich S, Garotta G, Musiani P. **Tumor rejection and immune memory elicited by locally released LEC chemokine are associated with an impressive recruitment of APCs, lymphocytes, and granulocytes**. *J Immunol*. 2000; 164(6): 3200-3206.

28. Huang B, Lei Z, Zhang GM, Li D, Song C, Li B, Liu Y, Yuan Y, Unkeless J, Xiong H, Feng ZH. **SCF-mediated mast cell infiltration and activation exacerbate the inflammation and immunosuppression in tumor microenvironment**. *Blood.* 2008; 112(4): 1269-1279.

29. De Bock K, Cauwenberghs S, Carmeliet P. **Vessel abnormalization: another hallmark of cancer? Molecular mechanisms and therapeutic implications**. *Curr Opin Genet Dev*. 2011; 21(1): 73-79.

30. Jung JE, Lee HG, Cho IH, Chung DH, Yoon SH, Yang YM, Lee JW, Choi S, Park JW, Ye SK, Chung MH. **STAT3 is a potential modulator of HIF-1-mediated VEGF expression in human renal carcinoma cells**. *FASEB J*. 2005; 19(10): 1296-1298.

31. Franco M, Roswall P, Cortez E, Hanahan D, Pietras K. **Pericytes promote endothelial cell survival through induction of autocrine VEGF-A signaling and Bcl-w expression**. *Blood*. 2011; 118(10): 2906-2917.

32. Hashimoto K, Matsumura I, Tsujimura T, Kim DK, Ogihara H, Ikeda H, Ueda S, Mizuki M, Sugahara H, Shibayama H, Kitamura Y, Kanakura Y. **Necessity of tyrosine 719 and phosphatidylinositol 3'-kinase-mediated signal pathway in constitutive activation and oncogenic potential of c-kit receptor tyrosine kinase with the Asp814Val mutation**. *Blood*. 2003; 101(3): 1094-1102.

33. Cavallo F, De Giovanni C, Nanni P, Forni G, Lollini PL. **2011: the immune hallmarks of cancer**. *Cancer Immunol Immunother*. 2011; 60(3): 319-326.

34. Furuya M, Yonemitsu Y, Aoki I. **Angiogenesis: complexity of tumor vasculature and microenvironment**. *Curr Pharm Des*. 2009; 15(16): 1854-1867.

35. Demuth PC, Min Y, Huang B, Kramer JA, Miller AD, Barouch DH, Hammond PT, Irvine DJ.**Polymer multilayer tattooing for enhanced DNA vaccination**. *Nature materials.* 2013; 12(4):367-76.

36. Goel S, Duda DG, Xu L, Munn LL, Boucher Y, Fukumura D, Jain RK. **Normalization of the vasculature for treatment of cancer and other diseases**. *Physiol Rev.* 2011; 91(3): 1071-1121.

37. Waskow C, Bartels S, Schlenner SM, Costa C, Rodewald HR. **Kit is essential for PMA-inflammation-induced mast-cell accumulation in the skin.** *Blood.* 2007; 109(12):5363-70.

38. Rathinavelu A, Narasimhan M, Muthumani P. **A novel regulation of VEGF expression by HIF-1α and STAT3 in HDM2 transfected prostate cancer cells.** *J Cell Mol Med.* 2012; 16(8):1750-1757.

39. Mitchem JB, Brennan DJ, Knolhoff BL, Belt BA, Zhu Y, Sanford DE, Belaygorod L, Carpenter D, Collins L, Piwnica-Worms D, Hewitt SM, Mallya Udupi G, Gallagher WM, Wegner C, West BL, Wang-Gillam A, Goedegebuure P, Linehan DC, Denardo DG. **Targeting tumor-infiltrating macrophages decreases tumor-Initiating cells, relieves immunosuppression and improves chemotherapeutic response.** *Cancer Res*. 2013; 73(3):1128-1141.

40. Chew HK, Barlow WE, Albain K, Lew D, Gown A, Hayes DF, Gralow J, Hortobagyi GN, Livingston R. **A phase II study of imatinib mesylate and capecitabine in metastatic breast cancer**: Southwest Oncology Group Study 0338. *Clin Breast Cancer*. 2008; 8(6):

511-515.

Figure 1

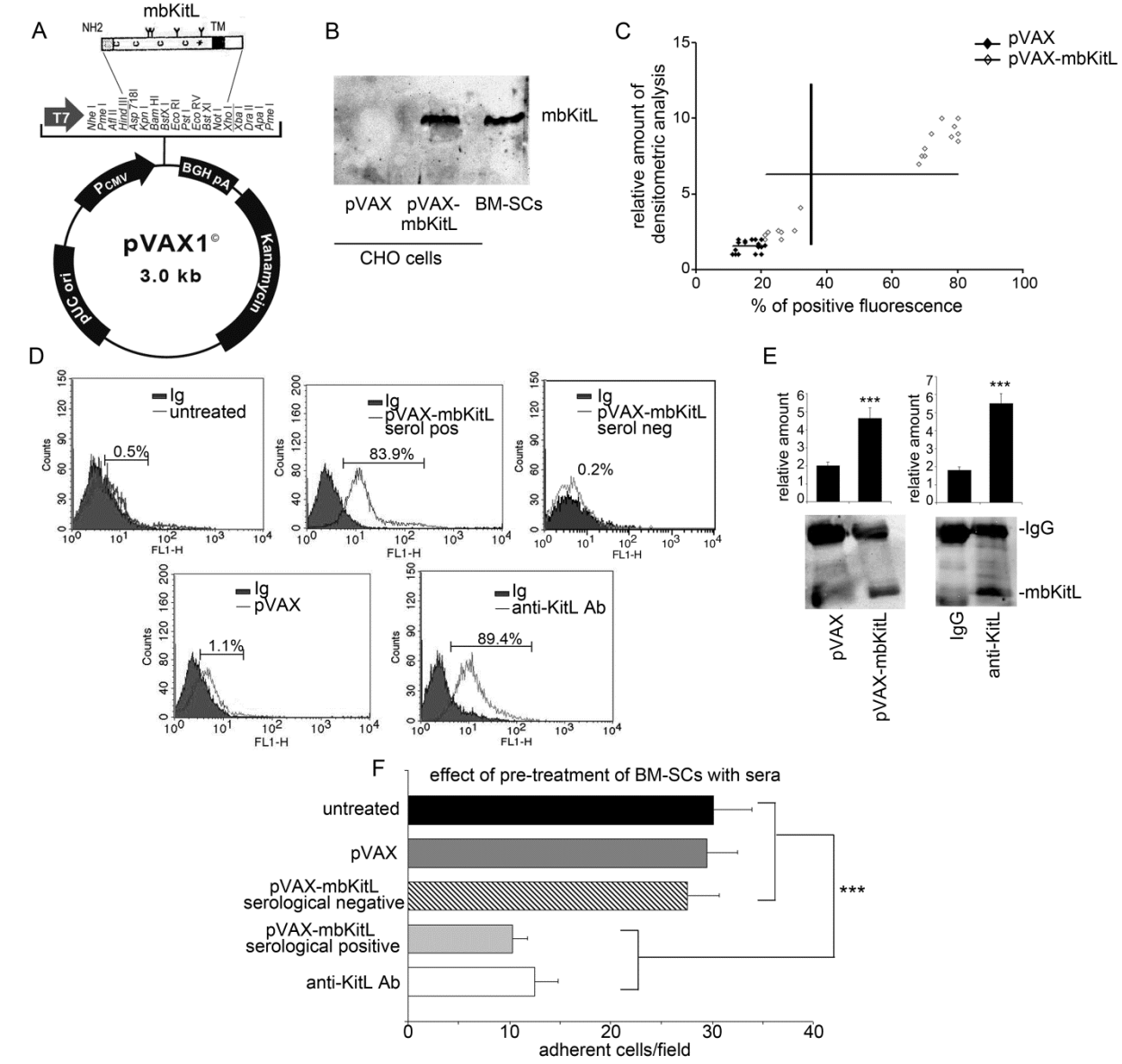

Figure 2

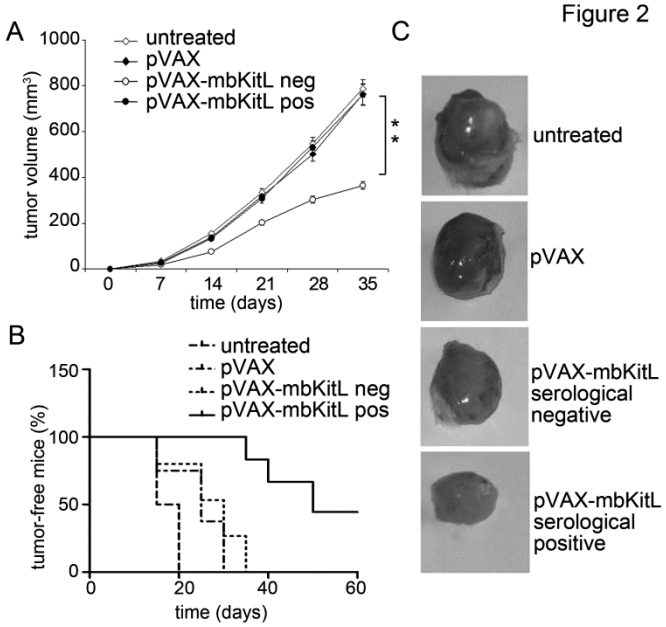
A
1000
800
600
400
200
0
tumor volume (mm3)
untreated
pVAX
pVAX-mbKitL neg
pVAX-mbKitL pos
**
0
7
14
21
28
35
time (days)
B
untreated
pVAX
pVAX-mbKitL neg
pVAX-mbKitL pos
150
100
50
0
tumor-free mice (%)
0
20
40
60
time (days)
C
untreated
pVAX
pVAX-mbKitL serological negative
pVAX-mbKitL serological positive

Figure 3

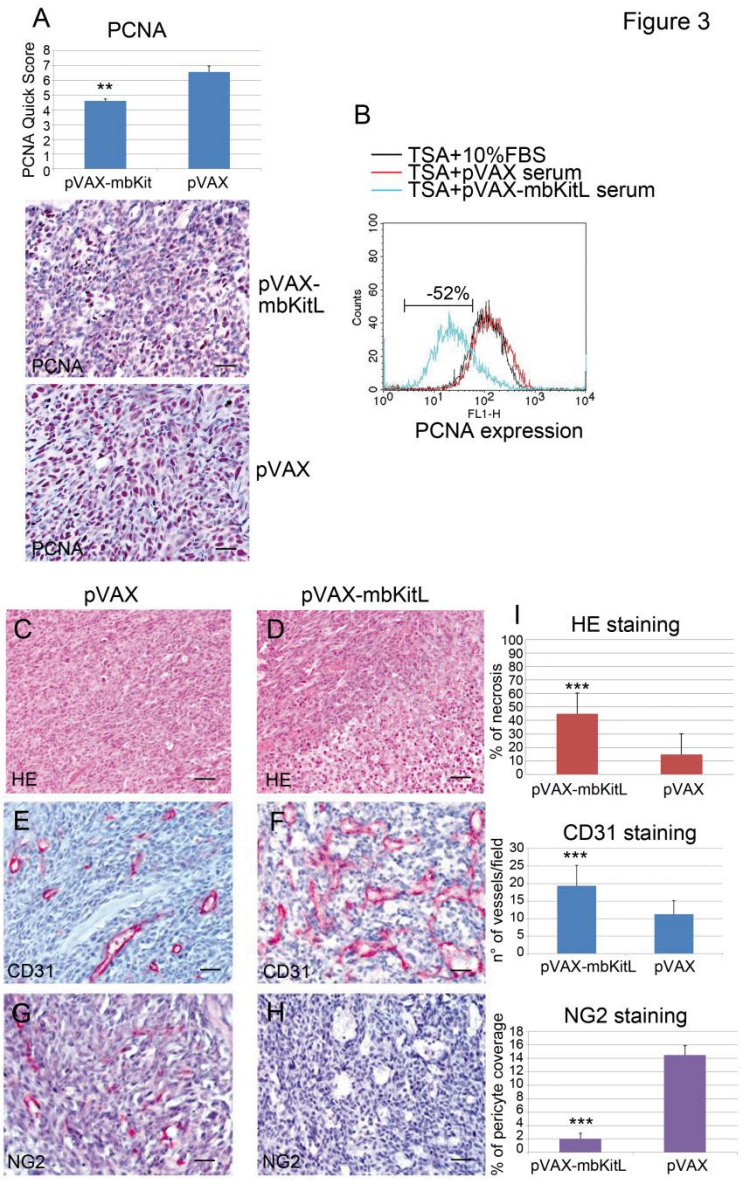
A
PCNA
PCNA Quick Score
**
pVAX-mbKit
pVAX
pVAX-mbKitL
PCNA
pVAX
PCNA
B
TSA+10%FBS
TSA+pVAX serum
TSA+pVAX-mbKitL serum
-52%
Counts
FL1-H
PCNA expression
pVAX
pVAX-mbKitL
C
HE
D
HE
I
HE staining
% of necrosis
***
pVAX-mbKitL
pVAX
E
CD31
F
CD31
CD31 staining
n° of vessels/field
***
pVAX-mbKitL
pVAX
G
NG2
H
NG2
NG2 staining
% of pericyte coverage
***
pVAX-mbKitL
pVAX

Figure 4

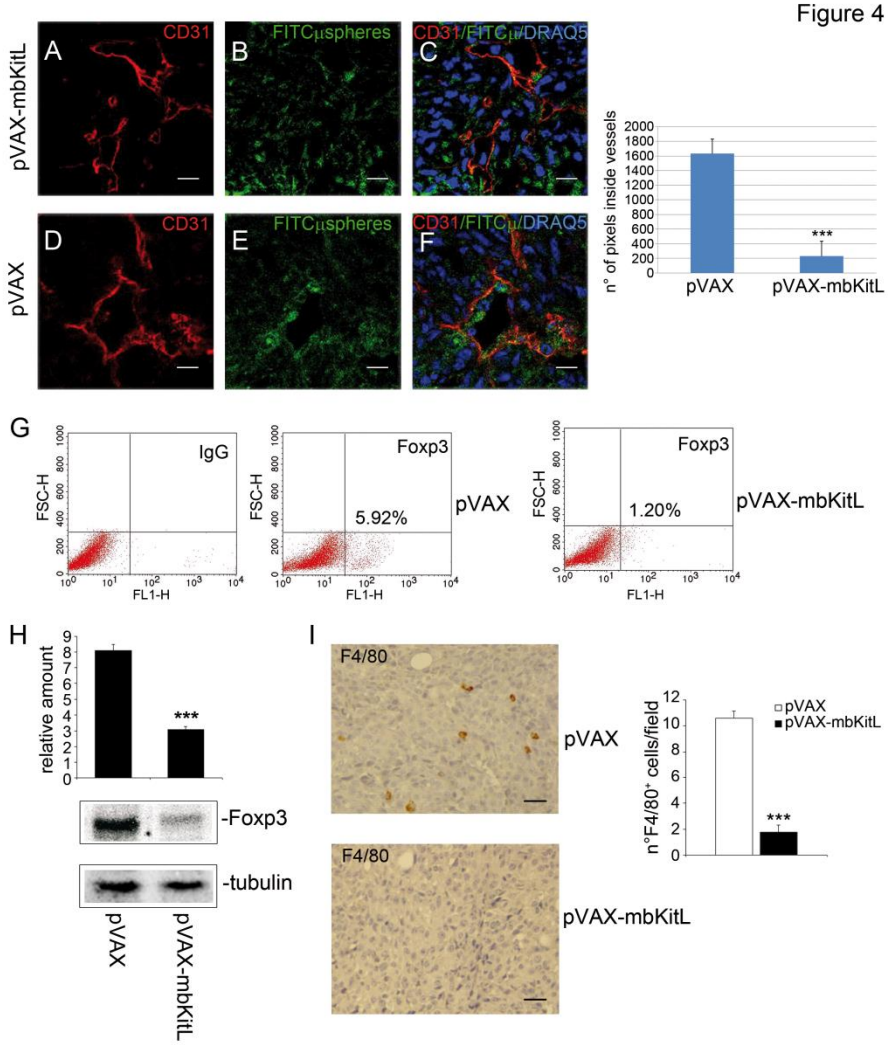
pVAX-mbKitL
pVAX
A
B
C
D
E
F
CD31
FITCμspheres
CD31/FITCμ/DRAQ5
n° of pixels inside vessels
2000
1800
1600
1400
1200
1000
800
600
400
200
0
***
pVAX
pVAX-mbKitL
G
IgG
Foxp3
5.92%
1.20%
pVAX
pVAX-mbKitL
FSC-H
FL1-H
H
relative amount
***
-Foxp3
-tubulin
pVAX
pVAX-mbKitL
I
F4/80
pVAX
pVAX-mbKitL
n°F4/80⁺ cells/field
pVAX
pVAX-mbKitL
***

Figure 5

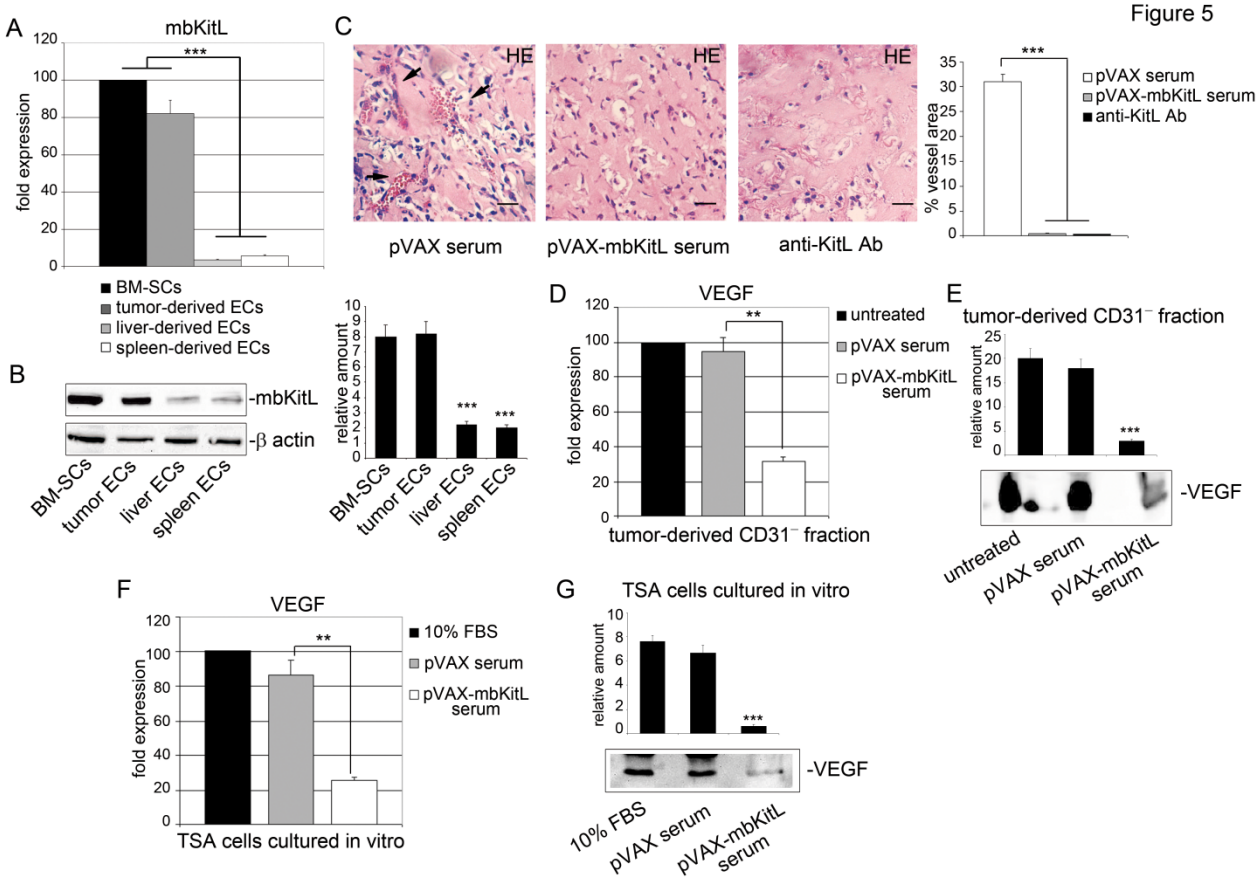
A
mbKitL
fold expression
BM-SCs
tumor-derived ECs
liver-derived ECs
spleen-derived ECs
B
-mbKitL
-β actin
BM-SCs
tumor ECs
liver ECs
spleen ECs
relative amount
C
HE
pVAX serum
pVAX-mbKitL serum
anti-KitL Ab
% vessel area
pVAX serum
pVAX-mbKitL serum
anti-KitL Ab
D
VEGF
fold expression
untreated
pVAX serum
pVAX-mbKitL serum
tumor-derived CD31⁻ fraction
E
tumor-derived CD31⁻ fraction
relative amount
-VEGF
untreated
pVAX serum
pVAX-mbKitL serum
F
VEGF
fold expression
10% FBS
pVAX serum
pVAX-mbKitL serum
TSA cells cultured in vitro
G
TSA cells cultured in vitro
relative amount
-VEGF
10% FBS
pVAX serum
pVAX-mbKitL serum

Figure 6

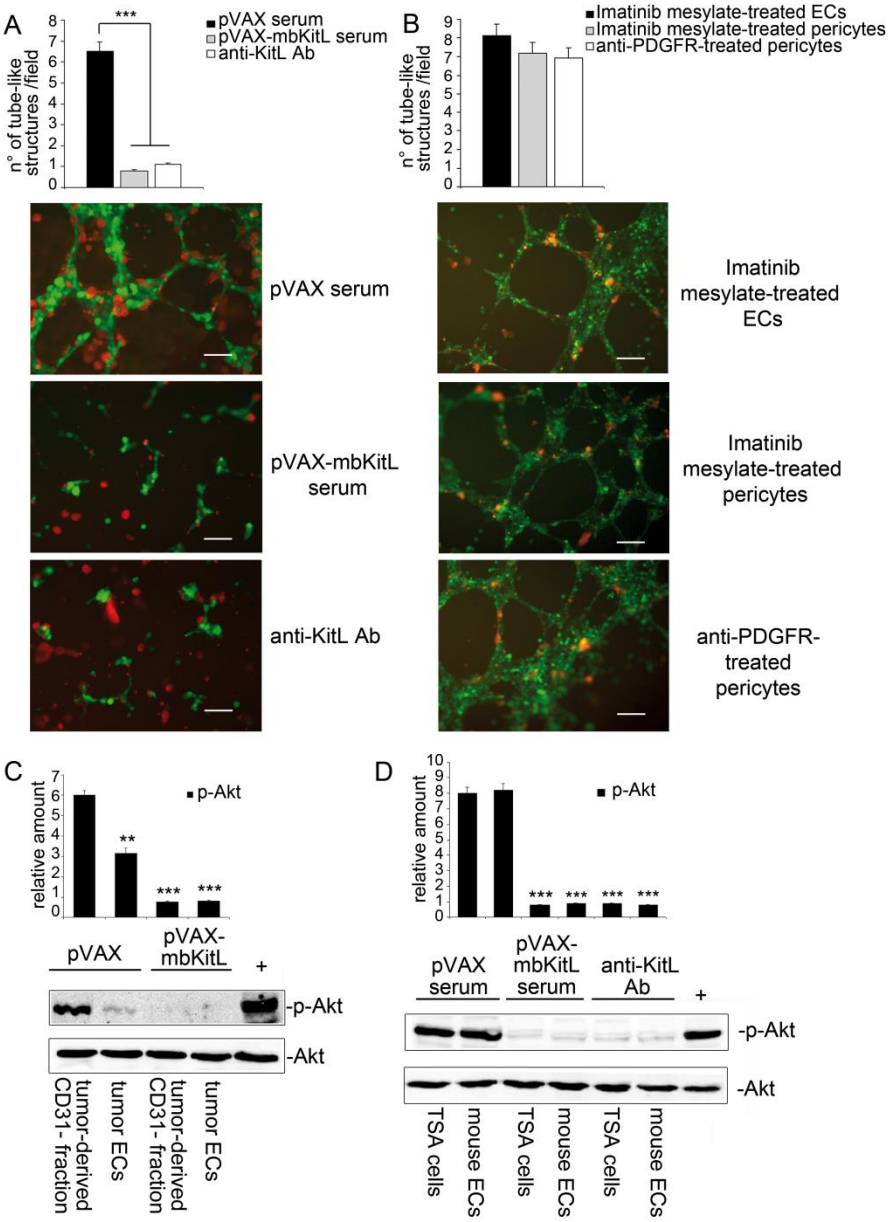
A
n° of tube-like structures /field
***
pVAX serum
pVAX-mbKitL serum
anti-KitL Ab
B
n° of tube-like structures /field
Imatinib mesylate-treated ECs
Imatinib mesylate-treated pericytes
anti-PDGFR-treated pericytes
pVAX serum
pVAX-mbKitL serum
anti-KitL Ab
Imatinib mesylate-treated ECs
Imatinib mesylate-treated pericytes
anti-PDGFR-treated pericytes
C
relative amount
p-Akt
**
***
***
pVAX
pVAX-mbKitL
+
-p-Akt
-Akt
tumor-derived CD31- fraction
tumor ECs
tumor-derived CD31- fraction
tumor ECs
D
relative amount
p-Akt
***
***
***
***
pVAX serum
pVAX-mbKitL serum
anti-KitL Ab
+
-p-Akt
-Akt
TSA cells
mouse ECs
TSA cells
mouse ECs
TSA cells
mouse ECs

Figure 7

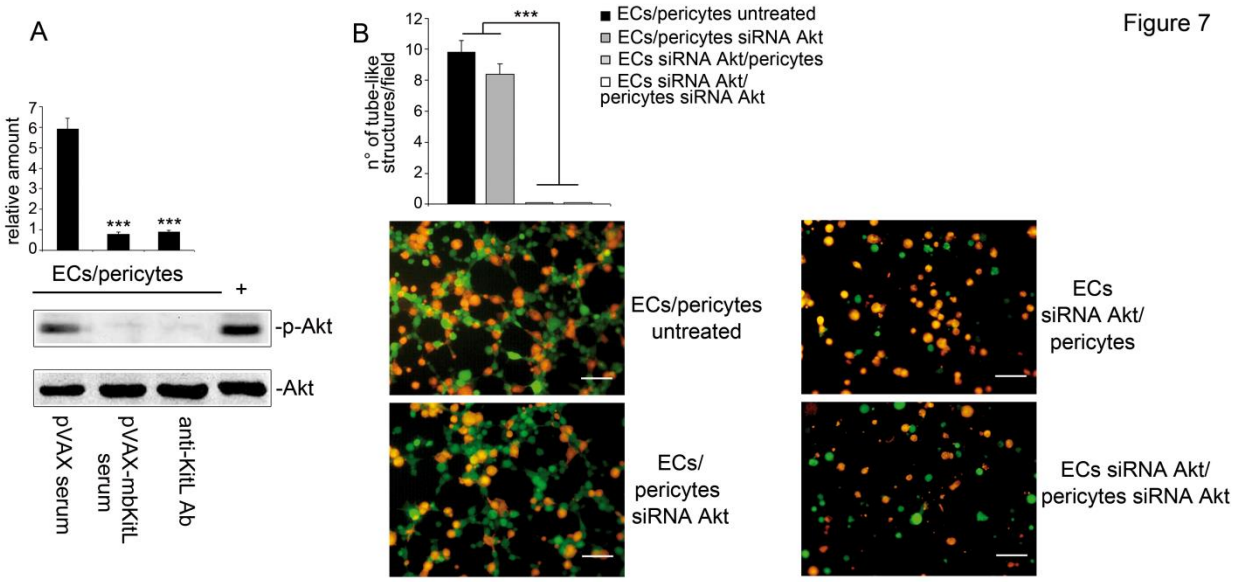

Figure 8

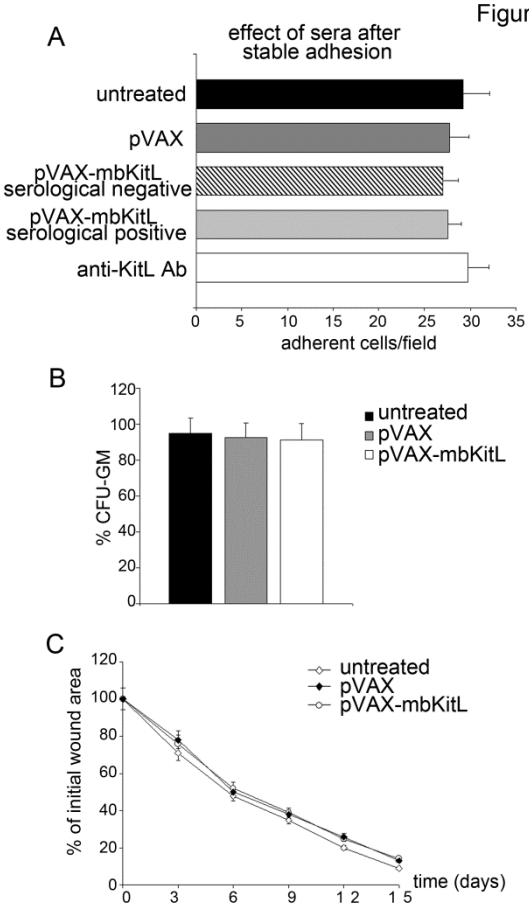

Figure S1

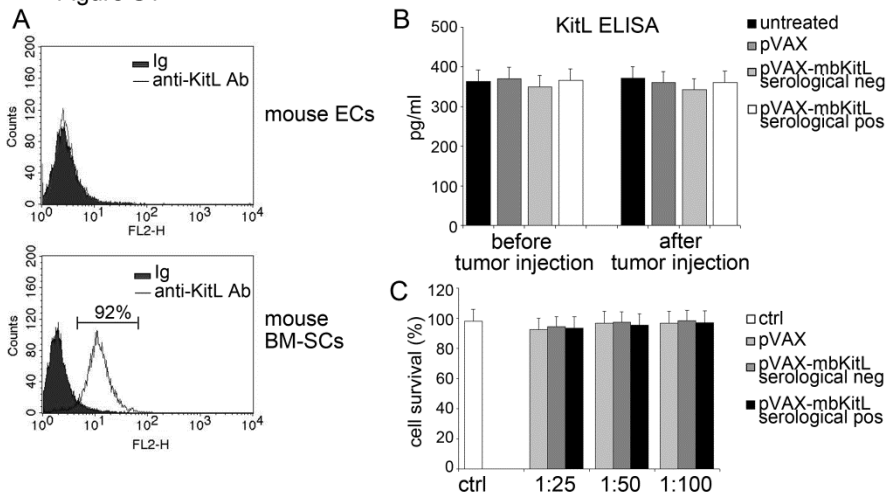

Figure S2

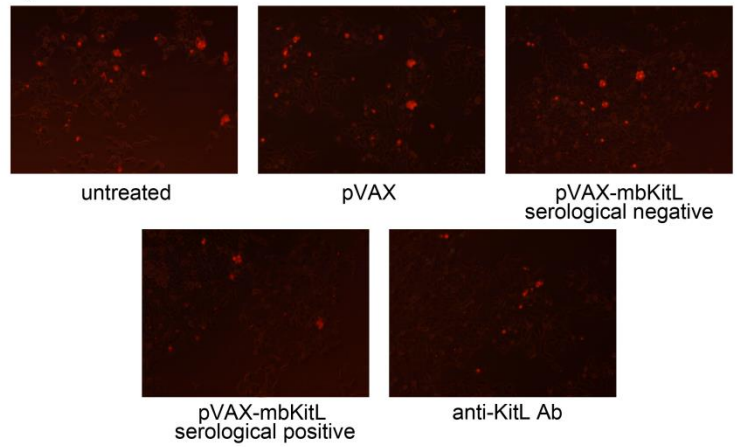

Figure S3

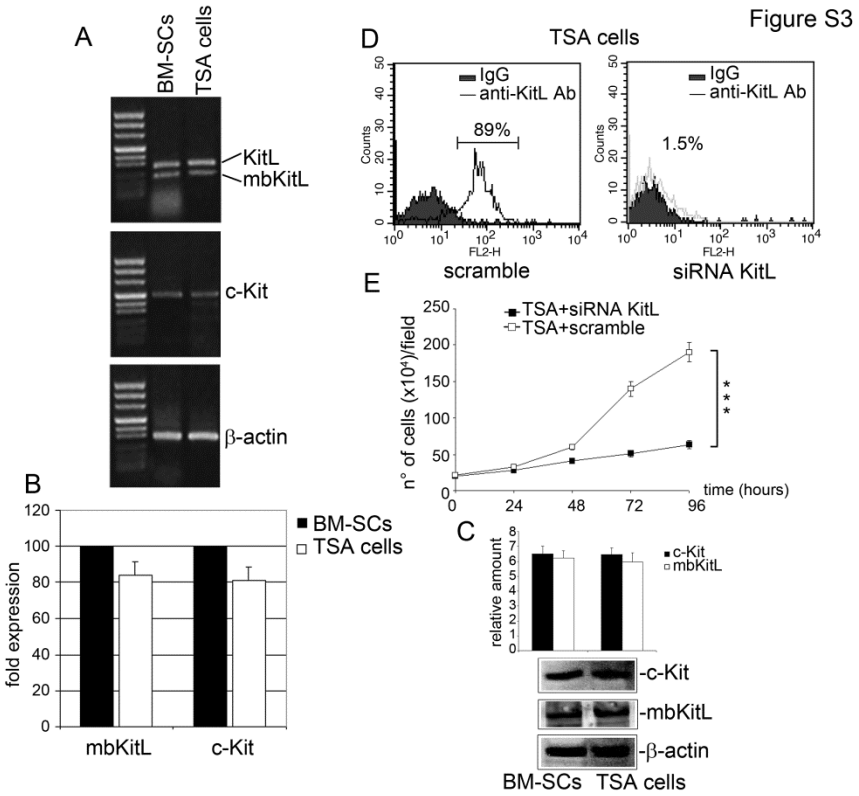

Figure S4

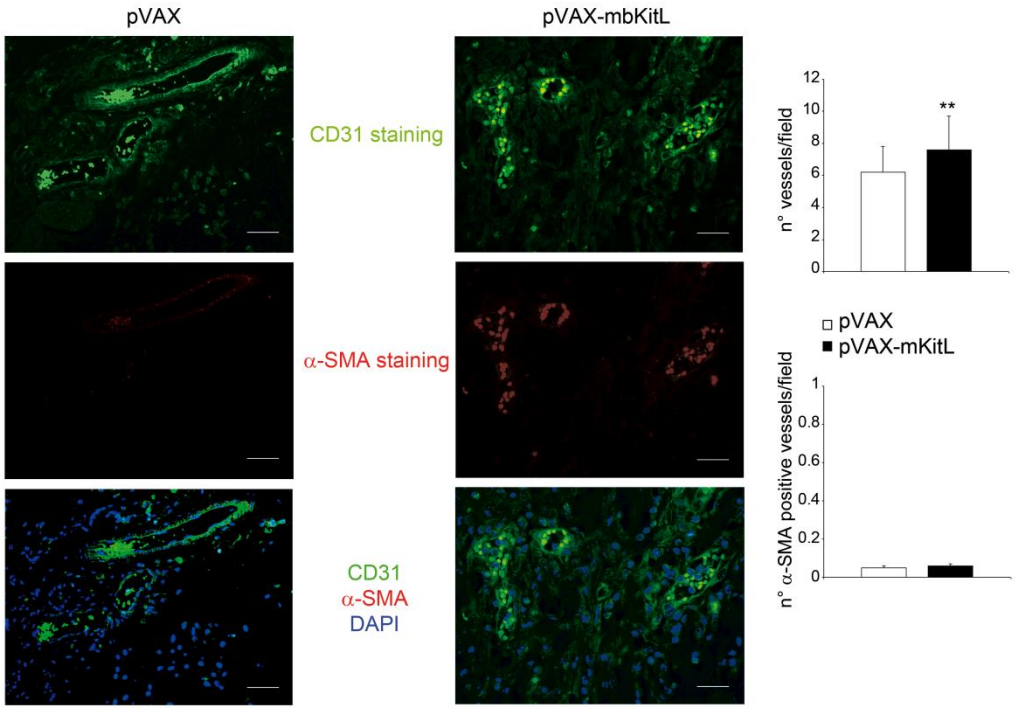

Figure S5

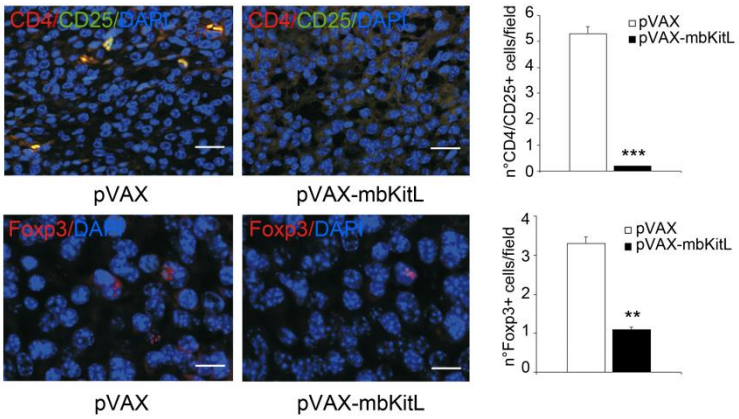

Figure S6

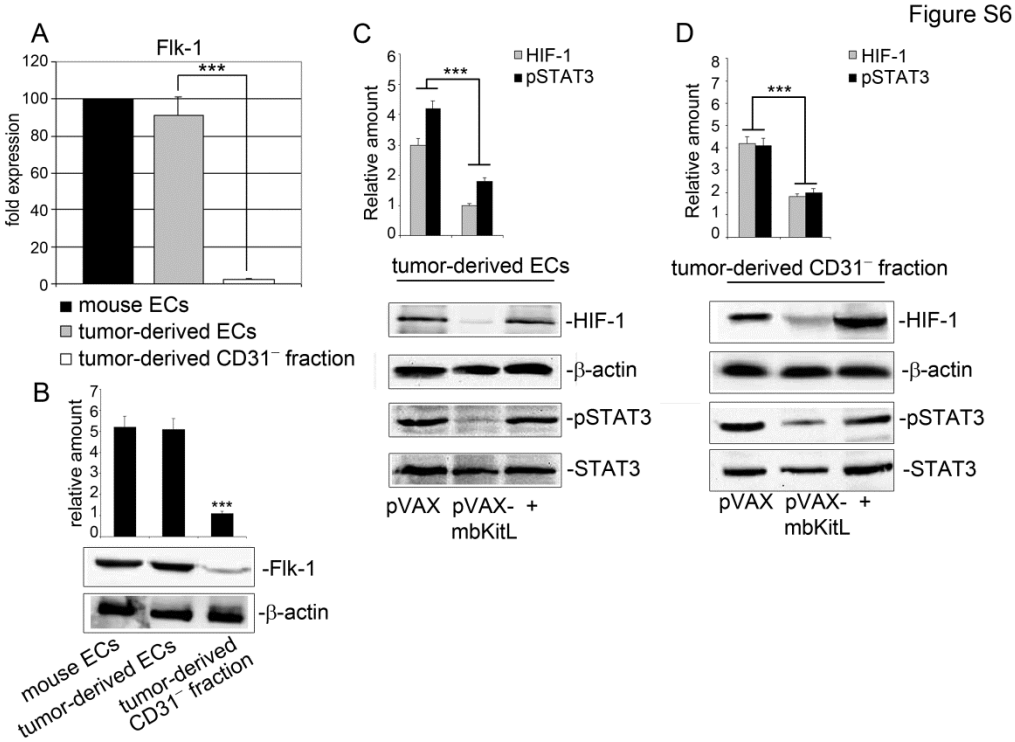

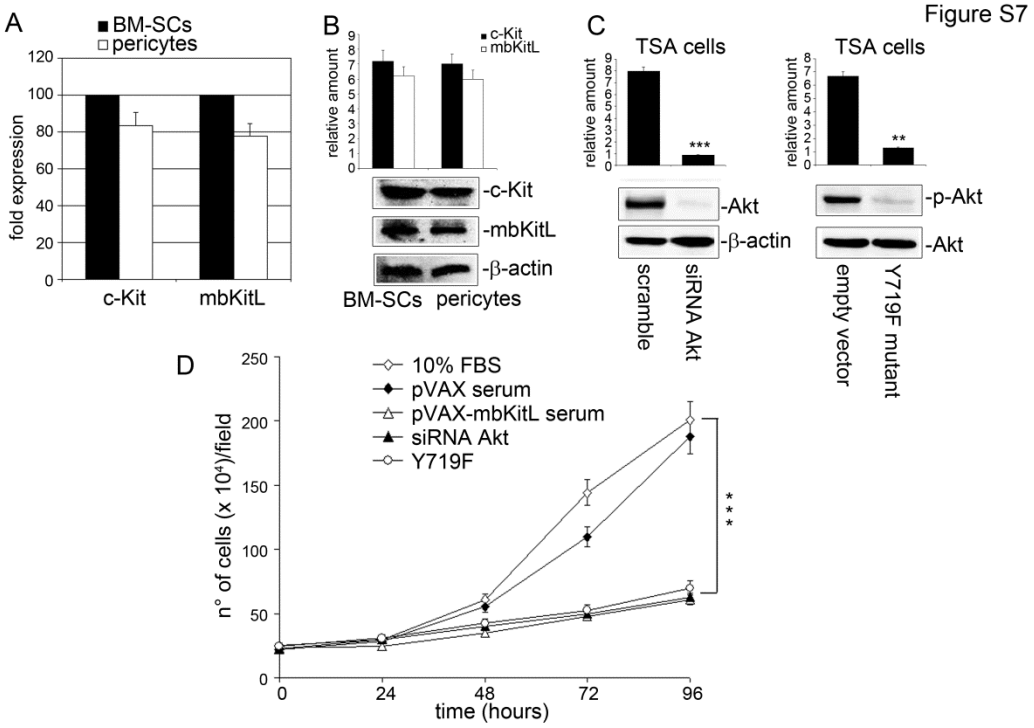

SUPPLEMENTARY INFORMATION

Supplementary Materials and Methods

Reagents and antibodies. RPMI, M199 and HBSS media, bovine serum albumin (BSA), trypsin, foetal bovine serum (FBS), collagenase IA and DAPI (4′,6-Diamidino-2-phenylindole dihydrochloride) were from Sigma-Aldrich (St Louis, MO, USA). EBM-2 medium was from Lonza (Walkersville, MD, USA). Matrigel Basement Membrane Matrix growth factor reduced and not growth factor reduced were from Biocoat, Becton Dickinson BD Labware, San Jose, CA, USA. Nitrocellulose filters, horseradish peroxidase-conjugated anti-rabbit or anti-mouse IgG, molecular weight markers and chemiluminescence reagents (ECL) were from Bio-Rad (Bio-Rad Laboratories, Hercules, CA). Anti-tubulin, anti-β-actin, anti-HIF1α, and anti-Kit ligand (KitL), raised against a epitope of mouse KitL, mapping at the N-terminus, cross-reacting with membrane bound and soluble KitL isoforms and with KitL of human origin (sc-1303), antibodies were obtained from Santa Cruz Biotechnology, Inc., Heindelberg, Germany. Anti-phospho-Akt (Ser-473/Thr-308), anti-Akt, anti-pSTAT3 and anti-STAT3 antisera were from Cell Signaling Technology (Beverly, MA, USA). Neutralizing rabbit polyclonal antisera to mbKitL and to PDGFRβ were from R&D Systems (Minneapolis, MN, USA). Secondary fluorochrome-conjugated antibodies were from Miltenyi Biotec Inc., Auburn, CA, USA. Anti-F4/80 antibody was from AbD Serotec, Oxford, UK. Anti-Foxp3, anti-α Smooth Muscle Actin (SMA) and anti-proliferating cell nuclear antigen (PCNA)

were from Abcam (Cambridge, UK). rmIL-3, rmIL-6, rmKitL an rhKitL were from R&D Systems. Imatinib mesylate was from Novartis (West Sussex, UK).

Cell cultures. ECs, used for in-vitro experiments, were isolated from human umbilical veins and cultured as previously described[1]. Mouse stromal cells (SCs) were obtained recovering total mouse bone marrow (BM) cells by flushing from femurs and tibias of Balb/c untreated mice and let to adhere to 6/well plates in presence of RPMI medium supplemented with 10% FBS. Non adherent mouse BM mononuclear cells (MNCs) were recovered and used as c-Kit expressing cells in the adhesion assay. Murine TSA cell line, derived from a spontaneously arising Balb/c mammary tumor, was kindly provided by Prof. S. Giordano and maintained in RPMI medium with 10% of FBS. Human tumor-derived endothelial cells (TECs), kindly provided by Prof. Camussi, were isolated and grown as previously described[2] and maintained in EBM-2 medium supplemented of 10% FBS. Human brain vascular pericytes (HBVP, SC1200, ScienCell, San Diego, CA, USA) were maintained in pericyte medium (ScienCell). Chinese hamster ovary (CHO) cell line was cultured in RPMI medium supplemented of 10% FBS. In selected experiments cells were treated as indicated and subjected to different experimental procedures as following described. Cell viability was evaluated by trypan blue at the end of each experiment.

Cell proliferation. TSA cell proliferative activity in response to pVAX and pVAX-mbKitL vaccination derived sera was assayed for indicated time intervals by direct cell count, by three individual operators in triplicate, as previously described[3]. Proliferation was also evaluated on TSA cells depleted of Akt or transfected with a c-Kit mutant, Y719F, unable to activate Akt[4] and reported in histograms as number ± SEM of cells per field (10X magnification).

Analysis of the immune response after DNA vaccination. To assess antibody generation in mice vaccinated with pVAX empty or pVAX-mbKitL vector or untreated for DNA vaccination, serum samples were collected by retro-orbital bleeding 15 days after the last immunization. Sera were centrifuged, dialyzed and analysed on mouse BM-SCs, expressing the mbKitL isoform. The cells were incubated with sera, with a isotype pre-immune IgG or with the anti-KitL antibody, recognizing the membrane bound isoform, used as control, for 30 minutes at 4°C. Then, they were washed twice in PBS and incubated for 30 minutes at 4°C with the secondary FITC-conjugated antibodies. The expression of mbKitL was evaluated by fluorescence activated cell sorting (FACS) analysis using FACS Calibur flow cytometer (BD Biosciences).

Histology, immunohistochemistry and immunofluorescence. Cryostatic sections of tumor samples were stained with hematoxylin/eosin or processed for immunohistochemistry (IH) or for immunofluorescence (IF). For the evaluation of vessels and pericytes, sections were incubated with rat anti-mouse antibodies against CD31 (BD Pharmingen, USA) and rabbit anti-mouse NG2 (Millipore, USA) for IH analysis or with anti-CD31 and rabbit anti-mouse αSMA for IF. Slides for IH were incubated with the appropriate biotinylated secondary antibody: goat anti-rat IgG or goat anti-rabbit IgG (Jackson ImmunoResearch Laboratories, Inc., West Grove, PA) at 1:500 for 30 minutes. Immunoreactive antigens were detected using NeutrAvidin^{TM} Alkaline Phosphatase Conjugated (Thermo Scientific-Pierce Biotechnology, Rockford, USA) and Vulcan Fast Red (Biocare Medical, USA). Slides for IF were incubated with the appropriate secondary FITC- or TRICT-conjugated antibodies. DAPI staining was used as nuclear marker. Fluorescent images were acquired with a Zeiss LSM 5 Pascal confocal laser-scanning microscope (Carl Zeiss, Jena, Germany) equipped with a helium/neon laser (543 mm), an argon laser (450-530 mm), and an EC planar Neofluar 40X/1.3 oil-immersion differential interference contrast objective lens. Images were analyzed using Zeiss LSM 5 version 3.2 software.

Quantitative studies of immunohistochemically stained sections were performed independently by two pathologists in a blind fashion. Ten microscopic fields in each sample were chosen for the determination of necrotic areas, vessels and pericytes. The expression of necrosis was defined as absent or scarcely, moderately or frequently.

For microvessel counts and pericytes, individual microvessels were counted under a microscope x400 field (5 random fields from each slide; x40 objective and x10 ocular lens, 0.180 mm2 per field). Microvessels distribution was evaluated considering their diameters, while pericytes count was performed comparing the percentages of NG2 positive cells in the two groups.

For the evaluation of proliferating cells in situ, sections were incubated with mouse antibody against PCNA (Clone PC10, Dako, USA), then incubated with the appropriate biotinylated secondary antibody MACH3-Mouse-Probe-RtU (Biocare Medical, USA). Immunoreactive antigens were detected using MACH3-Mouse-Polymer-RtU and Bajoran-Purple-Chromogen (Biocare Medical). Images were obtained from Leica DMRD-DC500. All pictures at 40X magnification.

The differences in PCNA expression in the two experimental groups were analyzed using our modified version of the quick-score[5]. The quick-score categories were based on both the intensity and the proportion of brown staining nuclei, counted in our modification, in 5 random fields from each slide at 400X magnification. The proportion of malignant cells staining positively throughout the section was termed category A and was assigned scores from 1 to 6 (1 =0-4%; 2= 5-19%; 3 = 20-39%; 4 = 40-59%; 5 = 60-79%; 6 = 80-100%). The whole section was scanned at low power in

order to determine the general level of intensity throughout. The average intensity, corresponding to the presence of negative, weak, intermediate, and strong staining, was given a score from 0 to 3, respectively, and termed category B. Category A was added to category B (A+B) to form an additive quick-score. Additive quick- scores from both groups were then compared.
For the evaluation of inflammatory cell infiltration: sections were incubated with rat anti-mouse F4/80 antibody and processed by IH. Immunoreactive antigens were detected using biotin/steptavidin system (Dako, Glostrup, Denmark).

EC and tumor cell isolation from tumor masses and ECs from mouse liver. Section of tumor masses were finely minced with scalpels and digested by incubation for 1h at 37°C in HBSS containing 0.1% collagenase IA. After washing in medium plus 10% BCS cell suspension was forced through a graded series of meshes to separate the cell component from stroma and aggregates. Cells were re-suspended and ECs were isolated via anti-mouse CD31 antibody coupled to magnetic beads, by magnetic cell sorting using the MACS system (Miltenyi Biotech, Auburn, CA). Briefly, cells were labeled with the anti-mouse CD31 antibody for 20 min and then were washed twice and re-suspended in MACS buffer (PBS without Ca2+ and Mg2+, supplemented with 1% BSA and 5 mM/L EDTA) at the concentration of 0.5×10^6 cells/80 μl. After washing, the cells were separated on a magnetic stainless steel wool column, according to manufacturer's instructions. Positive separated cells correspond to ECs, while negative separated cells have been considered mainly composed by tumor cells; both cell populations were recovered and used for qRT-PCR or Western Blot analysis. To verify the endothelial phenotype Flk1 mRNA expression was evaluated by qRT-PCR. Mice subjected to DNA vaccination and tumor challenge were also subjected to liver exportation. Liver samples were finely minced, digested and processed as above described. Cells were re-suspended and ECs were isolated by magnetic cell sorting via anti-mouse CD31 antibody microbeads (Miltenyi Biotech). Liver-derived ECs were also used in selected experiments and reported as mouse-derived ECs.

Cytofluorimetric analysis. FACS analysis was performed by FACS Calibur flow cytometer (BD Biosciences) on: (a) mouse ECs and BM-SCs to evaluate the mbKitL expression, using the commercial anti-KitL antibody cross-reacting with the membrane bound KitL isoform; (b) TSA cells cultured with or without 10% FBS or sera recovered from pVAX or pVAX-mbKitL vaccinated animals to evaluate PCNA expression: (c) cells derived from tumor digestion of immunized mice to evaluate nuclear Foxp3 expression: A total of 1×10^6 cells for each experimental group were treated with the primary antibodies or with a isotype pre-immune IgG for 30 minutes at 4°C,

washed twice in PBS and incubated for 30 minutes at 4°C with the secondary FITC- or PE-conjugated antibodies. To detect Foxp3 nuclear expression cells were previously permeabilized by perm buffer (eBioscience, San Diego, CA, USA).

In-vivo angiogenesis assay. For in-vivo angiogenesis assay SCID mice (four mice for each experimental group), purchased from Charles River Laboratories, were injected subcutaneously into the left flank with Matrigel matrix containing $2x10^6$ TECs in combination with the sera derived from pVAX or pVAX-mbKitL vaccination or the anti-KitL neutralizing antibody. Six days later, Matrigel plugs were recovered and fixed in 10% buffered formalin and embedded in paraffin for histological analysis. The vessel area and the total Matrigel area were planimetrically assessed from hematoxylin–eosin stained sections as previously described[3]. Only the structures possessing a patent lumen and containing red blood cells were considered vessels. Angiogenesis was expressed as the percentage ± SD of the vessel area to the total Matrigel area (% vessel area, 10X magnification). TEC-derived neoformed vessels were quantified using a human anti-CD31 antibody (Santa Cruz Biotechnology). Any stained CD31+ cell or CD31+ cell cluster, clearly separated from connective tissue elements, was considered as a single microvessel and counted, according to Weidner et al.[6]. Images were obtained from Leica DMRD-DC500.

Analysis of the medullar component. In order to exclude any effect on the medullar component of mice after DNA vaccination, BM cells, isolated by flushing of femurs and tibias of Balb/c mice, were cultured on a substrate of MethoCult semisolid methylcellulose (GF M3534, Stem Cells Technology, USA), with rmIL-3 (10 mg/ml), rmIL-6 (50 ng/ml) and rmKitL (10 ng/ml), in order to assess the integrity of the myeloid progenitors expressed as colony forming units (CFU-GM). Clonogenicity was expressed as percentage ± SD of colonies/CFU-GM colonies.

Tube-like structure formation assay. To analyze EC/pericyte interaction, 24-well plates were coated with basement Matrigel matrix (BD Biosciences). $4.5x10^4$ green pre-labelled ECs (CSFA vital dye, Molecular Probes, Invitrogen) and $2x10^4$ red pre-labelled pericytes (PKH26 vital dye, Sigma-Aldrich) were placed on top of the polymerized matrix, in presence or in absence of the sera derived from pVAX or pVAX-mbKitL vaccination or the anti-KitL neutralizing antibody. After 6h, tube-like structure formation was evaluated by three different operators (each experiment was performed in triplicate), counting 10 fields at 20X magnification. In selected experiments, where indicated, ECs or pericytes were pretreated for 1h at 37°C with the receptor tyrosine kinase pharmacological inhibitor, Imatinib mesylate (100 μM/L), or with a neutralizing anti-PDGFRβ

antibody (30 μg/ml). Alternatively ECs or pericytes depleted of Akt were used. Images were acquired by Zeiss LSM 5 Pascal confocal laser-scanning microscope (Carl Zeiss). ECs and pericytes were subsequently recovered from Matrigel matrix after digestion in HBSS containing 0.1% collagenase IA for 30 min at 37°C. The cells were washed in medium plus 10% BCS, filtered to physically separate the cell component from Matrigel matrix and then isolated by centrifugation. The cells were then used for Western Blot analysis.

Vessel permeability. Vessel permeability was investigated by injecting 50 nm fluorescent polymer microspheres (Duke Scientific, Palo Alto, CA) diluted in 0.9% NaCl (Sigma-Aldrich) to a volume of 100 μl into the tail vein 6 h before sacrifice. Tumors were then fixed in paraformaldehyde 1% for 1 h at 4°C, rinsed several times with PBS, infiltrated overnight with 30% sucrose in PBS at 4°C, embedded in Optimum Cutting Temperature (OCT; Bio Optica, Milan, Italy) compound and then frozen at -80°C. 4 μm thick sections were stained with anti-CD31 antibody and DRAQ5 (Alexis Biochemicals, San Diego, CA). Images were acquired by Zeiss Meta LSM 510. All pictures at 40X magnification.

Akt Silencing by small interfering RNAs (siRNA) and cell transfection. To obtain Akt inactivation, ECs, pericytes and TSA cells were transiently transfected with siRNA for Akt and with duplex siRNAs purchased by Qiagen (Valencia, CA, USA). Transfection was performed according to the vendor's instructions. 48h later whole cell extracts were processed. Cell viability was evaluated at the end of the experiments. TSA cells were also transiently transfected with a c-Kit mutant construct, containing a phenylalanine substitution at the tyrosine residue 719 (Y719F)[4], unable to activate Akt. Transfection was performed by the lipofectin method (Invitrogen).

Cytotoxicity test. To evaluate the cytotoxicity of sera collected from immunized mice, mouse BM-derived stromal cell monolayer was incubated with sera diluted at various concentrations in phosphate buffer (1:25, 1:50, 1:100) at 37°C for 4h. The cells were then detached with Trypsin, stained with Trypan Blue and viable cells were evaluated by a direct cell count (10 fields at 20X magnification per sample). Each experiment was performed in triplicate and count was performed by three different operators.

Western blot. Cells were lysed (50 mM Tris HCl [pH 8.3], 1% Triton X-100, 10 mM PMSF, 100 U/mL aprotinin, 10 μM/mL leupeptin), and protein concentration was obtained as previously described[1]. 50 μg of proteins were electrophoretically separated on SDS-polyacrylamide gels and

transferred to nitrocellulose membranes and revealed by chemiluminescence detection system (ECL). A time course experiment was performed on tumor cells and tumor-derived ECs treated with pVAX or pVAX-mbKitL vaccination derived sera or with the anti-KitL neutralizing antibody (40 μg/ml) (0-15min-30min-1h-2h) to detect p-Akt levels (data not shown). In the text was reported the p-Akt content at 2h.

RNA isolation and qualitative and quantitative Real-Time Polymerase Chain Reaction (RT-PCR). Total RNA was isolated using TRIzol Reagent (Invitrogen) from cells following the manufacturer's instructions. Single-stranded complementary DNA was synthesized from 50 ng of total RNA using a reverse transcription kit. Each complementary DNA generated was amplified by qualitative or quantitative RT-PCR in the Bio-Rad thermocycler (Hercules, CA, USA) and in the ABI PRISM 7700 (Applied Biosystems, Foxter Cyto, CA, USA), respectively. β-actin or GAPDH genes were used as standard reference. The relative expression of c-Kit and mbKitL was calculated by using comparative threshold cycle methods for qRT-PCR. c-Kit and mbKitL mRNA expression was determined using the following primer sequences: sense (5'-CCATTGATGCCTTCAAGGAC-3') and antisense (5'-GGCTGTCTCTTCTTCGAGTA-3') for mbKitL; sense (5'-AAGAGCTCGCAGAATCAGTGTTTGGGTCA-3') and antisense (5' TTGAGCTCCTTCAGAACTGTCAACAATTGG-3') for c-Kit. Vascular endothelial cell growth factor (VEGF) mRNA expression was also evaluated by qRT-PCR on tumor-derived cells or on TSA cells cultured in vitro as indicated using a specific Taq-Man Gene Expression assay (Applied Biosystems).

Adhesion assay. Adhesion of c-Kit-expressing cells (mouse BM-MNCs) to mbKitL-expressing cells (BM-SCs) was assayed in static conditions as previously described[7]. Briefly, BM-MNCs were labeled with the red fluorescent PKH26 vital dye and, after centrifugation at 1400 g for 10 min, were re-suspended in medium free containing 0.25% BSA. Cells were then added ($2x10^5$ cells/well) to confluent monolayer of BM-SCs. In selected experiments BM-SCs were treated or not with the sera derived from pVAX and pVAX-mbKitL vaccination or with anti-mbKitL antibody before addition of BM-MNCs. Co-cultures were thus incubated at 37°C for 4h and non-adherent cells were removed by washing three times with phosphate-buffered saline. To evaluate whether sera from pVAX-mbKitL vaccinated mice interfered with adhesion of c-Kit expressing cells to stromal cells, BM-MNCs were let to adhere to BM-SCs and incubated for 24h with sera. Samples were then fixed with 4% formaldehyde/ phosphate-buffered saline and observed under an epifluorescence microscope. Bound labelled c-Kit expressing cells were counted by three different operators in

triplicate and reported in histograms as number ± SEM of adherent cells per field (10 fields at 20X magnification per sample).

Wound model and analysis. The wound healing assay was performed as described by Botusan et al.[8]. Briefly, the hair of the flank of anesthetized animals (three mice per group) was depilated and rinsed with alcohol. Two full-thickness wounds were made on the dorsum on each side of midline using a 6-mm biopsy punch. For 2 days the mice received subcutaneous bupremorphine (0.03 mg/kg) twice of day to exclude any possible distress caused by surgical procedure. The wound images were recorded by a digital camera at the day of surgery and every other day. A circular reference was placed alongside to permit the correction for the distance between the camera and the animals. The wound area was calculated in pixels using the Nikon camera, corrected for the area of the circle reference and expressed as percentage ± SD of the original area.

ELISA assay. To detect KitL serum concentration in mice untreated or immunized with empty vector or pVAX-mbKitL construct before and after tumor injection, a competitive enzyme immunoassay (ELISA) was performed according to manufacturer's instruction (RayBiotech Inc., Norcross, GA, USA) using sera recovered by retro-orbital bleeding of mice. KitL levels were reported as pg/ml.

Statistical Analysis. All in vitro and in vivo results are representative of at least three independent experiments, performed in triplicate, unless otherwise indicated. Densitometric analysis using a Bio-Rad GS 250 molecular imager was used to calculate the differences in the fold induction of protein levels (Relative amount), normalized to β-actin or tubulin or Akt or STAT3 content, as indicated in the text, (*p< 0.05, **p< 0.01, ***p<0.001, statistically significant between experimental and control values) and each Western blot panel and relative densitometric histogram reported in the figures were representative of the results obtained in triplicate. Significance of differences between experimental and control values for both in vitro and in vivo experiments was calculated using analysis of variance with Newman-Keuls multicomparison test, and reported in detail in each figure legend. Differences in tumor-free survival (plotted as % tumor-free mice) were evaluated using the log-rank test/Kaplan-Meier survival plots. Quantitative analysis on immunohistochemical sections were performed as described in detail in the relative method section.

REFERENCES

1. Dentelli P, Del Sorbo L, Rosso A, Molinar A, Garbarino G, Camussi G, Pegoraro L, Brizzi MF. **Human IL-3 stimulates endothelial cell motility and promotes in vivo new vessel formation**. *J Immunol*. 1999; 163(4):2151-2159.
2. Bussolati B, Deambrosis I, Russo S, Deregibus MC, Camussi G. **Altered angiogenesis and survival in human tumor-derived endothelial cells**. *FASEB J.* 2003; 17(9):1159-1161.
3. Dentelli P, Del Sorbo L, Rosso A, Molinar A, Garbarino G, Camussi G, Pegoraro L, Brizzi MF. **Human IL-3 stimulates endothelial cell motility and promotes in vivo new vessel formation**. *J Immunol*. 1999; 163(4):2151-2159.
4. Hashimoto K, Matsumura I, Tsujimura T, Kim DK, Ogihara H, Ikeda H et al. **Necessity of tyrosine 719 and phosphatidylinositol 3'-kinase-mediated signal pathway in constitutive activation and oncogenic potential of c-kit receptor tyrosine kinase with the Asp814Val mutation**. *Blood*. 2003; 101: 1094-1102.
5. Detre S, Saccani Jotti G, Dowsett M. **A "quickscore" method for immunohistochemical semiquantitation: validation for oestrogen receptor in breast carcinomas**. *Clin Pathol*. 1995; 48(9): 876-878.
6. Weidner N, Semple JP, Welch WR, Folkman J. **Tumor angiogenesis and metastasis: correlation in invasive breast carcinoma.** *N Engl J Med*. 1991; 324: 1–7.
7. Biancone L, Cantaluppi V, Duò D, Deregibus MC, Torre C, Camussi G. **Role of L-selectin in the vascular homing of peripheral blood-derived endothelial progenitor cells**. *J Immunol*. 2004; 173(8):5268-5274.
8. Botusan IR, Sunkari VG, Savu O, Catrina AI, Grünler J, Lindberg S, Pereira T, Ylä-Herttuala S, Poellinger L, Brismar K, Catrina SB (2008) **Stabilization of HIF-1alpha is critical to improve wound healing in diabetic mice**. Proc Natl Acad Sci U S A 105(49):19426-19431.

Supplementary Figure Legends

Figure S1. mbKitL expression on mouse BM-SCs. (A) BM cells were isolated by flushing from femurs and tibias of wild-type Balb/c mice and let to adhere to select SCs. Cytofluorimetric analysis was performed on mouse-derived ECs and BM-SCs using a preimmune IgG antibody (IgG) (black peaks), as control, and the anti-KitL antibody (sc-1303), recognizing the membrane bound isoform. mbKitL (percentage±SD): mouse ECs, 0.1±0.2; anti-mbKitL, 92±3.6; ***p<0.001.
mbKitL vaccination does not affect KitL serum concentration in immunized animals. (B) ELISA assay was performed according to manufacturer's instructions to evaluate KitL concentration into the sera recovered from all mice untreated or immunized with pVAX and pVAX-mbKitL vaccines before and after tumor injection. Histogram reports KitL concentration (pg/ml) ± SD. **(C)** Sera recovered from untreated or vaccinated mice were diluted at various concentrations in phosphate buffer (1:25, 1:50, 1:100) and incubated with plated BM-SCs at 37° C for 4h. Sera cytotoxicity was evaluated by direct cell count of Trypan Blue stained viable cells. Cell survival is reported as percentage ± SD of viable cells. Data reported are representative of three independent experiments performed in triplicate, unless otherwise indicated.

Figure S2. mbKitL expression on TSA cells mediates cell proliferation. (A) mbKitL and c-Kit expression was evaluated by qualitative (upper panel) or quantitative (lower panel) RT-PCR on BM-SCs and TSA cells. Qualitative PCR underlined the presence of the two mRNA transcripts for KitL and mbKitL variant into the cells. Fold expression of mbKitL and c-Kit was normalized to β-actin (qualitative) or GAPDH (quantitative) content and was representative of three independent experiments performed in triplicate. **(B)** FACS analysis was performed on TSA cells silenced (siRNA KitL) or not (scramble) for KitL transcript using a preimmune IgG antibody (IgG) (black peaks), as control, and the anti-KitL antibody (sc-1303). ***p<0.001 mbKitL expression on scramble TSA cells 89±3.2% vs siRNA KitL TSA cells 1.5±2.5%. **(C)** Cell proliferation of TSA silenced or not for KitL, as above, and treated with pVAX- or pVAX-mbKitL-derived sera at different time intervals by a direct cell count. (***p<0.001 TSA cells+scramble vs TSA cells+siRNA KitL in presence of pVAX-mbKitL serum). Data reported are expressed as number±s.d. of cells per field (10X magnification). Data reported are representative of three independent experiments performed in triplicate.

Figure 3. Vessels in TSA-derived tumors do not express α-SMA positive cells. Tumor sections from pVAX- or pVAX-mbKitL-vaccinated mice were double stained with anti-mouse CD31 FITC-

conjugated and anti-mouse αSMA TRITC-conjugated antibodies. DAPI staining was used as nuclear marker. Histograms report the number±s.d. of vessels per field and the number±s.d. of aSMA positive cells per field. Scale bars indicate 100 μm (10X magnification). (*$p<0.05$, tumor vessels in pVAX-mbKitL vs in pVAX vaccinated mice).

Figure S4. Flk1 expression on tumor-derived ECs (A) ECs purified by anti-CD31 magnetic beads from tumor masses and tumor cells recovered after EC purification were subjected to qRT-PCR to detect Flk1 mRNA expression. Mouse- derived ECs were used as positive control. Fold expression of Flk1 was normalized to GAPDH content and was representative of three independent experiments performed in triplicate. **mbKitL vaccination reduces HIF-1 levels and STAT3 activation in tumor-derived cells.** Tumor-derived ECs (B), purified by anti-CD31 magnetic beads, and tumor cells (C), recovered after EC purification, from pVAX or pVAX-mbKitL mice were subjected to western blot to analyze HIF-1, β-actin, pSTAT3 and STAT3 content.

Figure S5. c-Kit and mbKitL are expressed by pericytes (A) mbKitL and c-Kit expression was evaluated by qRT-PCR on human-brain vascular pericytes cell line. Fold expression of mbKitL and c-Kit was normalized to GAPDH content and was representative of three independent experiments performed in triplicate. BM-SCs were used as positive control for c-Kit and mbKitL expression.
TSA cell transfection and TSA cell proliferation. (B, left panel) TSA cells transfected (48h) with: Akt siRNA or with the scrambled sequence (scramble) (left panel) or the Y719F c-Kit mutant or empty vector (right panel) were lysed and analyzed for p-Akt, Akt and β-actin content. **(C)** Proliferation of TSA cells treated with 10% FBS, pVAX- or pVAX-mbKitL-derived sera, or silenced for Akt was evaluated at different time intervals (as indicated) by a direct cell count. TSA cells previously transfected with the Y719F c-Kit mutant, unable to activate Akt, were also used. (***$p<0.001$, TSA cells+pVAX-mbKitL serum, Akt depleted cells and TSA transfected with Y719F c-Kit mutant vs TSA cells+ 10% FBS and TSA cells + pVAX serum). Data reported are expressed as number±SEM of cells per field (10X magnification). All data reported are representative of three independent experiments performed in triplicate.